JURNAL INTEGRASI PROSES

Website: http://jurnal.untirta.ac.id/index.php/jip

Submitted: 7 Maret 2021 ***Revised: 19 April 2021*** ***Accepted: 24 Juni 2021***

PYROLYSIS CARBONIZATION OF SAGO STARCH

Haryadi Wibowo[1*], Arenst Andreas Arie[2], Budi Husodo Bisowarno[2]
[1]Master student of chemical engineering, Parahyangan Catholic University, Indonesia
[2]Department of Chemical Engineering, Parahyangan Catholic University, Indonesia
[*]Email: wibowo588@gmail.com

Abstract

The need for batteries is increasing from time to time, the anode is the most important part in the battery, the amorphous carbon is very suitable for use as the anode for sodium ion batteries (SIB). Amorphous carbon is obtained through the process of carbonization of hydrocarbons. Research on the synthesis of hydrocarbon carbonization from sago starch is still rarely done. This study aims to determine the carbon characteristics of sago starch treated with nitrogen doping according to the SIB anode by paying attention to morphology, size distribution, material structure, material composition, and the distance between layers. The carbonization method used in this study is the pyrolysis process at a temperature of 900°C for 1 hour. Experimental variations were carried out through direct pyrolysis process with variations of urea to starch 3:1, 2:1, and pure starch. The experimental results were analysed using SEM (EDS) and XRD. The results showed that the pyrolysis process treated with nitrogen with a ratio of urea 3:1 had an interlayer distance of 0.353304 nm, 2: 1 interlayer 0.368059 nm, and pure sago starch 0.390178 nm. This value indicates that carbon is a non-graphite material (> 0.3354 nm). Carbon produced from pyrolysis produces carbon which is amorphous and has a similar shape, which is like wood. The most suitable carbon used as anode for SIB battery is DHCD 2:1.

Keywords*: SIB, pyrolysis, nitrogen, SEM, XRD*

1. INTRODUCTION

Indonesia is an archipelagic country that has many sources of wealth that can be used as an energy source. These sources include tropical climates, volcanoes, and plant diversity that have the potential to be processed into renewable energy. The sun always rises every day in tropical countries, so sunlight can be used as a solar power plant (Ramadhan, Diniardi, & Mukti, 2016). Mount Merapi can be used as a geothermal power plant (Khadijah, 2018). Some mountainous areas have wind that can be used as wind power plants (Maychel, Mangindaan, & Tumaliang, 2019). Plant diversity can be converted into bio-energy through a fermentation process into alcohol, biodiesel, and biogas. It can be used as a fuel source.

Renewable energy sources have advantages over fossil fuels. Fossil energy sources have weaknesses including limited energy sources, and produce exhaust gases that can pollute the environment. Renewable energy has several disadvantages, including the need for storage sources because the use of electrical energy is increasing over time.

Batteries are one of the electrical energy storage technologies. Energy storage in the form of batteries consists of primary batteries (single use) and secondary batteries (rechargeable batteries) (Besenhard, 2008). Primary batteries are batteries that can only be used once and are commonly used for electronic devices such as clocks, tv remotes, ac remotes, and radios. Secondary batteries are batteries that can be used repeatedly by adding negative electrons to the battery. Secondary batteries are more widely used in various fields such as electric cars, laptops, cameras, and renewable energy storage.

The secondary battery consists of several parts including the positive electrode (cathode), negative electrode (anode), and electrolyte (Besenhard, 2008). Secondary batteries that are widely developed include lithium ions battery (LIB) and sodium ion battery (SIB). The invention of lithium ions batteries changed the battery industry because lithium ions batteries can store battery capacities up to 2-3 times higher per unit weight (Winter, Besenhard, Spahr, & Novak, 1998). Lithium ions batteries use graphite as the anode and

$LiCO_2$ as the cathode (Titirici, 2013). The content of lithium in the world is so limited that it cannot cover the needs of the whole world. The limited lithium content causes the price of lithium batteries to be expensive. The working principle of SIB is the same as LIB because it involves the conduction of alkaline ions in the medium (Dou et al., 2019). Substitution of LIB with SIB is an opportunity to be developed, because the sodium content in Indonesia is very abundant. Sodium cannot form intercalations with graphite (Sangster & Diffusion, 2007), so it takes another anode that can form intercalations with sodium, namely carbon which is amorphous. Besides not forming intercalation, graphite also has a small interlayer distance of 0.335 nm which can inhibit the intercalation process (Górka, Vix-Guterl, & Matei Ghimbeu, 2016). the sodium ion battery intercalation process can take place if the interlayer distance is 0.37 nm (Liu et al., 2019). The working principle of SIB uses the principle of conductivity. The conductivity can be increased by the addition of nitrogen doping.

Carbon is usually taken from hydrocarbon compounds. Carbohydrates are hydrocarbons found in plants, carbohydrates consist of several types including monosaccharides, disaccharides, oligosaccharides, and polysaccharides (Azhar, 2016). Starch is a polysaccharide found in plants. The starch component consists of amylose, linear component, and amylopectin (Koswara, 2009), Amylose is a homopolysaccharide that is not branched. In contrast to amylopectin, amylopectin is a homopolysaccharide that has branches. Amylose and amylopectin form complex structures called starch grains (Mischnick & Momcilovic, 2010). Amylose is composed of α-D-glucose monomer residues connected by α- (1 → 4) glucose bonds, namely glycoside bonds between C-1 from one glucose molecule and C-4 from glucose (Bertoft, 2017), Amylopectin is a polymer of α- (1 → 4) glucose units with α- (1 → 6) glucose units as side chains (Herawati, 2016). Amylose can form amorphous structures so they can be used as SIB electrodes. The starch carbonization process can be carried out with the direct carbonization stage, namely direct burning of starch, pyrolysis is a direct combustion of starch without oxygen. Pyrolysis is a stage in the carbonization process of incomplete combustion of plant, animal, and mineral materials containing carbon (Haji, 2006; Paris, Zollfrank, & Zickler, 2005). Pyrolysis is also an endothermic process that thermally converts carbohydrates into valuable fuels and chemicals in the absence of oxygen through rapid heating (Nizamuddin et al., 2018). The pyrolysis process uses a temperature of 200°C to 1000°C in the absence of oxygen. The pyrolysis process can increase the surface area, improve the quality of the carbon content, and the pore continuity. The pyrolysis reaction pathway includes cracking, decarboxylation, hydrocracking, hydrodeoxygenation and hydrogenation (Dou et al., 2019).

The purpose of this study was to determine the characterization of carbon by direct combustion and the effect of adding nitrogen doping to its characterization. The nitrogen doping used in pyrolysis is urea. The characterization was carried out in the form of SEM analysis to determine the morphology of the carbon surface structure and carbon size distribution, and XRD which resulted in the interlayer distance on the carbon.

2. MATERIALS AND METHODS

The raw materials are sago starch which is used as a carbon source and urea which is used as nitrogen doping on carbon. The furnace used is a tube-shaped furnace with nitrogen flowing which serves to remove the oxygen content in the furnace.

Figure 1. Tubular furnace

The carbonization treatment process scheme is shown in Figure 2. The figure in part (a) (DHC) produced by the scheme of the carbonization process carried out without the addition of urea by adding 16 grams of starch. Figure part (b) (DHCD 2:1) produced by the scheme of the carbonization process carried out with the addition of nitrogen, the addition of nitrogen in the form of adding 10.67 grams of urea to 5.33 grams of sago starch. The figure in section (c) (DHCD 3:1) produced by the scheme of the carbonization process carried out with the addition of nitrogen, the addition of nitrogen in the form of the addition of 12 grams of urea added to 4 grams of sago starch. A mixture of 16 grams of sago starch was put into a crucible and then burned in a tube-shaped furnace at a temperature of 900oC for 1 hour. The carbon from the furnace is then crushed and then weighed.

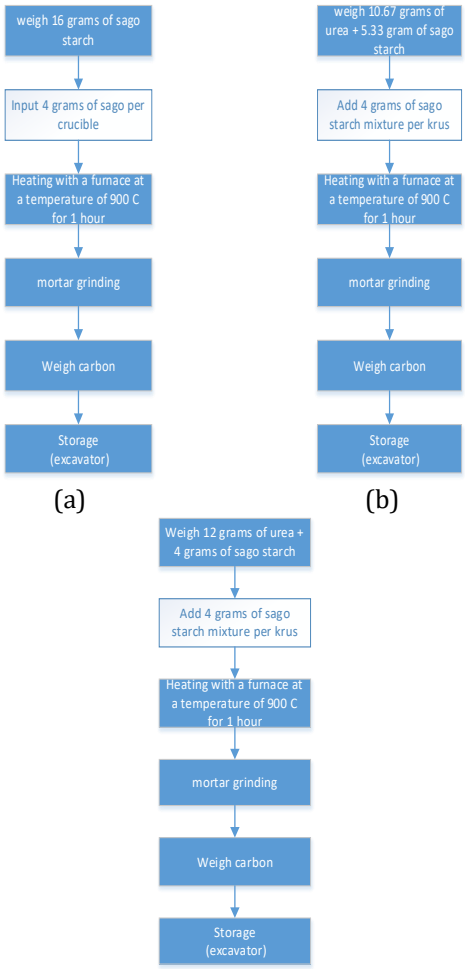

Figure 2. Direct carbonization (a) without doping, (b) doping 2: 1, and (c) doping 3: 1

2.1 SEM Analysis

SEM analysis serves to determine the morphological structure, particle size distribution, and the average diameter of carbon and hard carbon particles. Determination of the particle size distribution and the mean particle diameter with the help of the ImageJ application, the type of SEM tool used is SEM SU3500.

2.2 XRD Analysis

XRD analysis serves to determine the carbon interlayer distance. XRD results are read using the Origin Lab application so that the θ value and the XRD reflection field can be found. Calculation of interlayer distance, intercrystallite distance, layer arrangement height, and lateral length of hard carbon follows Bragg and Scherrer's law with the Equation (Khosravi, Bashirpour, & Nematpour, 2014):

$$d = \frac{\lambda}{2 \times \sin(\theta)}, hkl = (002)\ atau\ (100) \quad (1)$$

$$L_{c(002)} = \frac{K_c \times \lambda}{\beta \times \cos(\theta)} \quad (2)$$

$$L_{a(100)} = \frac{K_a \times \lambda}{\beta \times \cos(\theta)} \quad (3)$$

with:

λ = X-ray wavelength (0.15406)
θ = Bragg angle at the diffraction peak (radians)
d = Xray reflection plane distance (nm)
$L_{(002)}$ = L_c = layer arrangement height (side)
$L_{(100)}$ = L_a = lateral length (nm)
$d_{(002)}$ = d_c = intercrystallite and micro crystallite distance (nm)
$d_{(100)}$ = d_a = starling interlayer (nm)
β = full width at half maximum (FWHM) (radians)
K_c = 0.9: K_a = 1.84 (Khosravi et al., 2014)

3. RESULT AND DISCUSSION

3.1 SEM-EDX

SEM-EDX generated through the pyrolysis process with 3 variations of doping produced in Figure 3. shows the shape of carbon like a wood chip. The carbon size is still large, and for DHC carbon doping the particle size has started to decrease. The diagonal size of the average carbon length of DHC, DHCD 2:1, and DHCD 3:1 is 29.07 µm, 13,79 µm, and 14,87 µm.

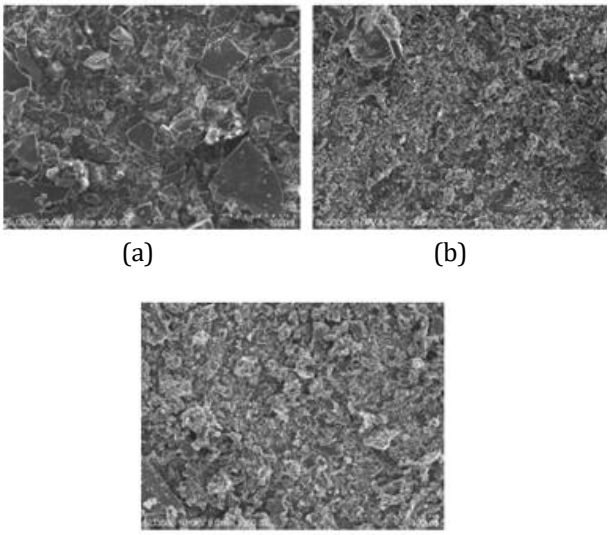

Figure 3. Morphology hard carbon at temperature 900°C (a) DHC (b) DHCD 2:1 (c) DHCD 3:1

The morphology of carbon contained in Figure 3, the distribution of carbon can be determined with the help of the Image j application. The results of the Image J application are then made a carbon particle distribution graph. Particle distribution can be seen in Figure 4. Figure 4 illustrates the distribution of DHC without doping which has a large size in contrast to carbon doped with smaller particle size. The distribution of particles in DHC is located on a diagonal of length between 20-30 µm, for the size of DHCD 2:1 and DHCD 3:1 have the same diagonal size between 10-20 µm. From this it explains that nitrogen doping reduces the size of carbon. The smaller the size of the carbon, the higher the surface area of interaction with the carbon, so it can increase the battery capacity. SEM-EDS analysis produces data in the form of hard carbon composition that has been processed as listed in Table 1.

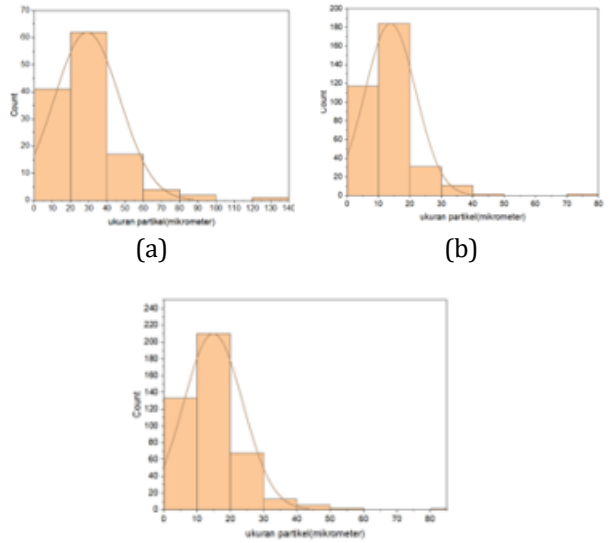

(a) (b)

(c)

Figure 4. The distribution of particles (a) DHC (b) DHCD 2:1 (c) DHCD 3:1

Table 1. Direct hard carbon composition

Element	Weight		
	DHC	DHCD 2:1	DHCD 3:1
C	84.8	84.5	84.27
N	0	0	0
O	11.05	10,19	10.44
Na	0.17	0.47	1.3
Al	0.12	0.14	0.14
Si	0.53	0.25	0.13
K	2.14	1.45	2.93
Fe	0.28	1.33	0.79
Ni	0.91	1.67	0
Total	100	100	100

Based on table 1, nitrogen doping is not properly formed and the composition contained in the carbon is almost similar. The content of the three carbon sources is 84 %. In direct combustion, there are several impurities including O, Na, Al, Si, K, Fe, and Ni. The higher the carbon content, the better the quality of the carbon, so DHC is very good for use as a battery anode.

3.2 XRD

The results of the XRD analysis are then processed using the origin lab application to determine the 2θ peak by plotting the graph between 2θ and Y, Figure 5. XRD analysis results processed using origin.

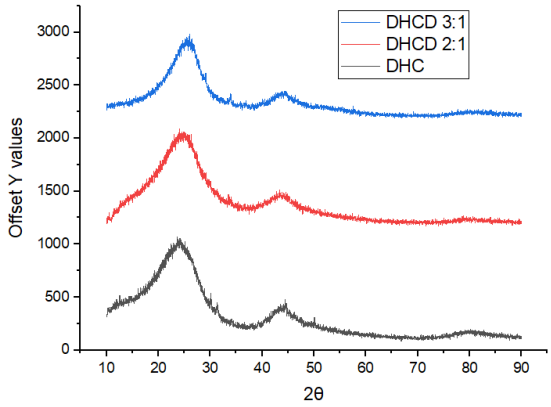

Figure 5. Direct XRD analysis hard carbon

The direct hard carbon samples obtained were characterized using XRD in order to determine the crystalline structure of DHC. Based on Figure 5, it can be seen that DHC has 2 peaks at 2θ values of 22°-23° in the plane (002) and 43°-45° in the plane (100). Fields (002) and (100) indicate that DHC is a carbon with amorphous characteristics and an irregular structure (Hu, Cheng, Ren, Wang, & Ren, 2019).

Based on the XRD carbon graph in Figure 5, then the theta (002) and theta (100) peaks are looked for which are then processed to determine the interlayer distance between the carbons, and the intercrystallite distance Table 2. describes the XRD results to find the interlayer.

Table 2. Results of bragg and scherrer XRD analysis

Result	DHC	DHCD (2:1)	DHCD (3: 1)
2θ (002) (°)	22.76341	24.15146	25,17625
2θ (100) (°)	44.47412	43.75175	44.31832
dc (002) (nm)	0.390178	0.368059	0.353304
Lc (002) (nm)	0.583909	0.813365	1.172018
da (100) (nm)	0.203469	0.206659	0.204148
La (100) (nm)	1.930598	2.257898	3.407690

Based on Table 2 with the Bragg equation, the interlayer distance (dc) and intercrystallite distance (da) are obtained, and intercrystallite distance (da), the location of the peak value 2θ (002) is at an angle of 22°-25° and the location of the peak value 2θ (100) is located at an angle of 43°-43.5°. At DHC, the interlayer distance is 0.39 nm, followed by DHCD 2: 1 of 0.368 nm, and DHCD 3:1 of 0.353 nm as listed in table 1, for dc values in DHC higher than the theoretical minimum value of anode sodium ion battery is 0.37 nm, the process of insertion Na^+ ions into DHC without doping are appropriate (Liu et al., 2019). The carbon composition regarding the crystalline and amorphous content resulting from the XRD analysis can be seen in Table 3.

Table 3. Crystallinity of direct hard carbon

Sample	DHC	DHCD 2:1	DHCD 3:1
% crystallinity	34.6	25.8	37.8
% amorphous	65.4	74.2	62.2

Table 3 explains that direct hard carbon has a lower crystal content than amorphous carbon. Based on table 32, the direct hard carbon content without doping at 900^{o}C was 34.6 %, at DHCD (2:1) the crystal value decreased to 25.8 %. whereas in DHCD (3:1) the crystal value increased again to 37 %. Based on this, it can be explained that urea can interfere with the pyrolysis combustion process. Meanwhile, the carbon expected for the battery electrode is the carbon with the highest amorphous value.

Amorphous properties are preferred for the manufacture of SIB due to the higher conductivity of the material, more stability, higher electrochemical performance compared to graphite (Chen et al., 2019). If the bonds between layers are weak, the carbon will easily form graphite (soft carbon). Conversely, if the carbon bonds are strong, it will be difficult to form graphite even though pyrolysis is carried out at high temperatures (hard carbon) (Irisarri, Ponrouch, & Palacin, 2015). The composition of each carbon is presented in table 3. So that the most suitable carbon to be used as anode carbon is DHCD2:1.

4. CONCLUSION

The carbon produced from pyrolysis produces almost the same shape, which is like chopped wood. Hard carbon directly from sago starch does not form microspheres. Amorphous characteristics are formed with a small amount of crystallinity. The addition of nitrogen doping has an impact on decreasing the distance between the carbon layers. The addition of urea causes the size of the hard carbon particles to instantly become smaller and reduces the distance between the carbons. The more urea is added, the interlayer distance decreases. Carbon from direct carbonization produces an amorphous type of carbon with an interlayer length of > 0.33354 nm so it is very suitable to replace graphite as anode of lithium ions batteries, Direct hard carbon without doping can be used as anode of Sodium ion batteries, because hard carbon has an interlayer distance greater than 0.37 nm. (Liu et al., 2019)

5. REFERENCES

Azhar, M. (2016). Biomolekul sel: karbohidrat, protein, dan enzim. In: UNP Press.

Bertoft, E. (2017). Understanding starch structure: Recent progress. Agronomy, 7(3), 56.

Besenhard, J. O. (2008). Handbook of battery materials: John Wiley & Sons.

Chen, X., Zheng, Y., Liu, W., Zhang, C., Li, S., & Li, J. (2019). High-performance sodium-ion batteries with a hard carbon anode: transition from the half-cell to full-cell perspective. Nanoscale, 11(46), 22196-22205.

Dou, X., Hasa, I., Saurel, D., Vaalma, C., Wu, L., Buchholz, D., Passerini, S. (2019). Hard carbons for sodium-ion batteries: Structure, analysis, sustainability, and electrochemistry. Materials Today, 23, 87-104 %@ 1369-7021.

Górka, J., Vix-Guterl, C., & Matei Ghimbeu, C. (2016). Recent progress in design of biomass-derived hard carbons for sodium ion batteries. C—Journal of Carbon Research, 2(4), 24.

Haji, A. G. (2006). Pembuatan arang dari sampah organik dengan cara karbonisasi menggunakan reaktor pirolisis. Jurnal Purifikasi, 7(2), 139-144 %@ 2598-3806.

Herawati, H. (2016). Potensi pengembangan produk pati tahan cerna sebagai pangan fungsional. Jurnal Penelitian dan Pengembangan Pertanian, 30(1), 31-39 %@ 2541-0822.

Hu, L., Cheng, G., Ren, J., Wang, F., & Ren, J. (2019). Conformal carbon coating on hard carbon anode derived from propionaldehyde for excellent performance of lithium-ion batteries. Int. J. Electrochem. Sci, 14, 2804.

Irisarri, E., Ponrouch, A., & Palacin, M. R. (2015). Hard carbon negative electrode materials for sodium-ion batteries. Journal of The Electrochemical Society, 162(14), A2476 %@ 1945-7111.

Khadijah, N. S. (2018). Analisis Pembangunan Pembangkit Listrik Tenaga Panas Bumi (PLTP) Melalui Insentif Fiskal dalam Mendukung Ketahanan Energi Indonesia. Ketahanan Energi, 3(2).

Khosravi, M., Bashirpour, N., & Nematpour, F. (2014). Synthesis of hard carbon as anode material for lithium ion battery.

Koswara, S. (2009). Teknologi modifikasi pati. Teknol. Pangan, 1-32.

Liu, J., Zhang, Y., Zhang, L., Xie, F., Vasileff, A., & Qiao, S. Z. J. A. M. (2019). Graphitic carbon nitride (g-C3N4)-derived N-rich graphene with tuneable interlayer distance as a high-rate anode for sodium-ion batteries. 31(24), 1901261.

Maychel, R., Mangindaan, G. M. C., & Tumaliang, H. (2019). Perencanaan Pembangunan Pembangkit Listrik Tenaga Bayu Di Likupang. Jurnal Teknik Elektro dan Komputer, 8(1), 15-20 %@ 2685-2368X.

Mischnick, P., & Momcilovic, D. (2010). Chemical structure analysis of starch and cellulose derivatives. In Advances in carbohydrate chemistry and biochemistry (Vol. 64, pp. 117-210 %@ 0065-2318): Elsevier.

Nizamuddin, S., Siddiqui, M. T. H., Mubarak, N. M., Baloch, H. A., Mazari, S. A., Tunio, M. M., . . . Riaz, S. (2018). Advanced nanomaterials synthesis from pyrolysis and hydrothermal carbonization: A review. Current Organic Chemistry, 22(5), 446-461 %@ 1385-2728.

Paris, O., Zollfrank, C., & Zickler, G. A. (2005). Decomposition and carbonisation of wood biopolymers—a microstructural study of softwood pyrolysis. Carbon, 43(1), 53-66 %@ 0008-6223.

Ramadhan, A. I., Diniardi, E., & Mukti, S. H. (2016). Analisis desain sistem pembangkit listrik tenaga surya kapasitas 50 WP. Jurnal Teknik, 37(2), 59-63.

Sangster, J. J. J. o. P. E., & Diffusion. (2007). C-Na (carbon-sodium) system. 28(6), 571-579.

Titirici, M.-M. (2013). Sustainable carbon materials from hydrothermal processes: John Wiley & Sons.

Winter, M., Besenhard, J. O., Spahr, M. E., & Novak, P. (1998). Insertion electrode materials for rechargeable lithium batteries. Advanced materials, 10(10), 725-763 %@ 0935-9648.